Dalton Transactions

ROYAL SOCIETY OF CHEMISTRY

COMMUNICATION

View Article Online
View Journal

Cite this: DOI: 10.1039/d1dt01799c

Received 2nd June 2021,
Accepted 8th June 2021

DOI: 10.1039/d1dt01799c

rsc.li/dalton

Mechanistic insights into Ni-catalyzed hydrogen atom transfer (HAT)-triggered hydrodefluorination of CF_3-substituted alkenes†

Jiandong Guo,[a,b] Dongju Zhang[b] and Xiaotai Wang *[a,c]

We report the first computational study on a nickel hydride HAT-initiated catalytic reaction, a novel hydrodefluorination of CF_3-substituted aryl alkenes to afford *gem*-difluoroalkenes. This study provides detailed mechanistic insights into the reaction, including HAT from NiH to C=C, a carbon radical rebound to nickel to facilitate chemoselective defluorination, and a two-state reactivity of Ni(II) enabling σ-bond metathesis with $PhSiH_3$ to regenerate the catalyst. The findings can have implications for developing new metal hydride HAT-initiated reactions.

There has been intense interest recently in metal hydride-mediated hydrogen atom transfer (HAT) to a C=C bond to generate a carbon-centered radical for Markovnikov-selective alkene hydrofunctionalization under mild conditions and with the tolerance of various functional groups.[1–4] The Norton group has recently achieved a breakthrough in this active area of research, reporting an unprecedented nickel hydride HAT-initiated catalytic hydrodefluorination of CF_3-substituted alkenes to form *gem*-difluoroalkenes, as shown in Scheme 1.[5] The *gem*-difluoroalkene moiety is found in a series of bioactive compounds and known as a bioisostere of the carbonyl group with increased metabolic stability.[6] Norton's reaction provides a new and viable approach to synthesize *gem*-difluoroalkenes, and it also represents a significant advance in the area of C–F bond activation through hydrodefluorination, considering that previous metal-promoted hydrodefluorination reactions were limited to aryl or alkenyl C–F bonds.[7]

Norton *et al.* proposed a HAT-initiated mechanistic outline based on the trapping of the radical **R1**• with TEMPO and other observations (Scheme 2 and Fig. S1†).[5] The Ni(II) hydride complex **CAT1** transfers a H atom to the alkene substrate **S1**, generating **R1**• while converting to the Ni(I) complex **A**. The abstraction of an F atom from **R1**• by **A** gives the product and forms the Ni(II) fluoride complex **B** that reacts with the hydrosilane to regenerate **CAT1**.

In contrast to the intense experimental activity, there are only a few reports of (combined) computational studies on metal hydride HAT-initiated reactions, which deal with cobalt or iron hydride species and alkene hydrogenation, polymerization, or cross-coupling reactions.[8–11] The novel NiH-mediated HAT-initiated hydrodefluorination of CF_3-substituted alkenes attracted our interest. With **CAT1** being a known and well-defined nickel hydride complex,[12] the reaction is well-suited for computational investigation. We have carried out extensive density functional theory (DFT) calculations by considering the mechanistic suggestions in Scheme 2 and other possibilities.

Here, we wish to report a detailed plausible mechanism and discuss our new findings in the hope of providing useful insights for the further development of nickel hydride HAT-initiated hydrodefluorination and other reactions.

We began our studies by optimizing **CAT1** in both the singlet and triplet spin states, and the singlet is more stable as

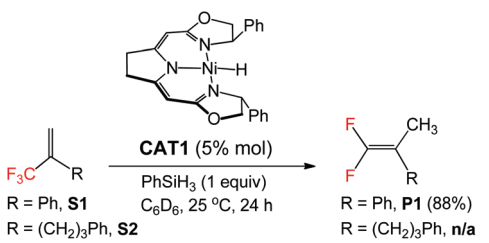

Scheme 1 Ni-catalyzed hydrodefluorination of CF_3-substituted aryl alkenes.

[a]*Hoffmann Institute of Advanced Materials, Postdoctoral Innovation Practice Base, Shenzhen Polytechnic, 7098 Liuxian Boulevard, Nanshan District, Shenzhen 518055, P. R. China*
[b]*Institute of Theoretical Chemistry, School of Chemistry and Chemical Engineering, Shandong University, Jinan 250100, P. R. China*
[c]*Department of Chemistry, University of Colorado Denver, Campus Box 194, P. O. Box 173364, Denver, Colorado 80217-3364, USA.*
E-mail: xiaotai.wang@ucdenver.edu

†Electronic supplementary information (ESI) available: Computational methods, additional computational results, benchmark DLPNO-CCSD(T) results of key structures, and Cartesian coordinates. See DOI: 10.1039/d1dt01799c

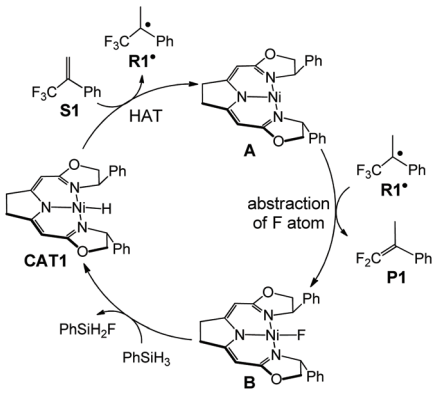

Scheme 2 Mechanistic outline proposed by experimentalists.

expected (Fig. 1). An open-shell transition state (TS) is required for a direct HAT from the Ni^{II}–H moiety of **CAT1** to the C=C bond of substrate **S1**. Indeed, we traced the open-shell singlet ^{OS}**TS1** that is 13.3 kcal mol^{-1} relative to **CAT1**. ^{OS}**TS1** contains an incipient organic radical with a spin density of −0.21 on the tertiary carbon and an emerging Ni(I) doublet complex with a spin density of 0.26 on the nickel center. The two spins are antiferromagnetically coupled, making a net open-shell singlet structure. A triplet transition state could not be found, but it could be ruled out because the triplet precursor ^{3}**CAT1** is already higher than ^{OS}**TS1** by 4.1 kcal mol^{-1}. An alternative HAT pathway would be through the C=C insertion into the Ni^{II}–H bond (*i.e.*, hydrometallation), followed by the homolysis of the Ni–C bond.[13] We located **TS2** for the hydrometallation, and then ruled out this pathway by considering that **TS2** is higher than ^{OS}**TS1** by 9.8 kcal mol^{-1}. Thus, the HAT process takes place through ^{OS}**TS1**, which is consistent with previous computational studies that found open-shell singlet transition states for Co^{III}–H HAT to C=C reactions.[8,11]

^{OS}**TS1** proceeds to the Ni(I) doublet complex ^{2}**IM1** and the organic radical **R1**$^{\bullet}$. For the evolution of **R1**$^{\bullet}$, we first considered ^{2}**IM1** abstracting an F atom directly from **R1**$^{\bullet}$, and located both the triplet and open-shell singlet pathways. The triplet pathway goes through the precursor complex ^{3}**IM2** and transition state ^{3}**TS3** and leads to ^{3}**IM4** and the hydrodefluorination product; the open-shell singlet pathway is less favorable (Fig. S2†). Nevertheless, we found a lower-energy pathway through the radical rebound to the Ni(I)[14] species ^{2}**IM1** *via* ^{3}**TS$_{REB}$** to form a more stable Ni(II) complex ^{3}**IM3**, followed by β-fluoride elimination[15] *via* ^{3}**TS4** to deliver the product. Because ^{3}**TS3** is higher than ^{3}**TS$_{REB}$** by 4.2 kcal mol^{-1}, the direct F abstraction pathway can be ruled out. We also considered and ruled out the higher-energy singlet counterparts of ^{3}**IM3** and ^{3}**TS4** (Fig. S3†).

The ^{3}**IM4** to **IM4** spin crossover *via* **MECP1** (minimum energy crossing point 1) is downhill by 1.4 kcal mol^{-1}, but the subsequent concerted interchange (or σ-bond metathesis) of **IM4** with $PhSiH_3$ would encounter **TS5** that is 31.0 kcal mol^{-1} above **IM4**. This high barrier would stop the reaction. Thus, **IM4** reverts to ^{3}**IM4**, and the σ-bond metathesis proceeds *via* the triplet ^{3}**TS5** that is lower than **TS5** by 19.5 kcal mol^{-1}. This regenerates the catalyst in the triplet state ^{3}**CAT1**, which then proceeds *via* **MECP2** to singlet **CAT1** to close the catalytic cycle. Therefore, the calculations suggest a two-state reactivity[16] of Ni (II) for the σ-bond metathesis step. We examined the bonds being formed or broken in the four-membered ^{3}**TS5** and **TS5** and their precursors (Fig. 1). The most significant difference is observed in the change of the Ni–F bond: it must be stretched

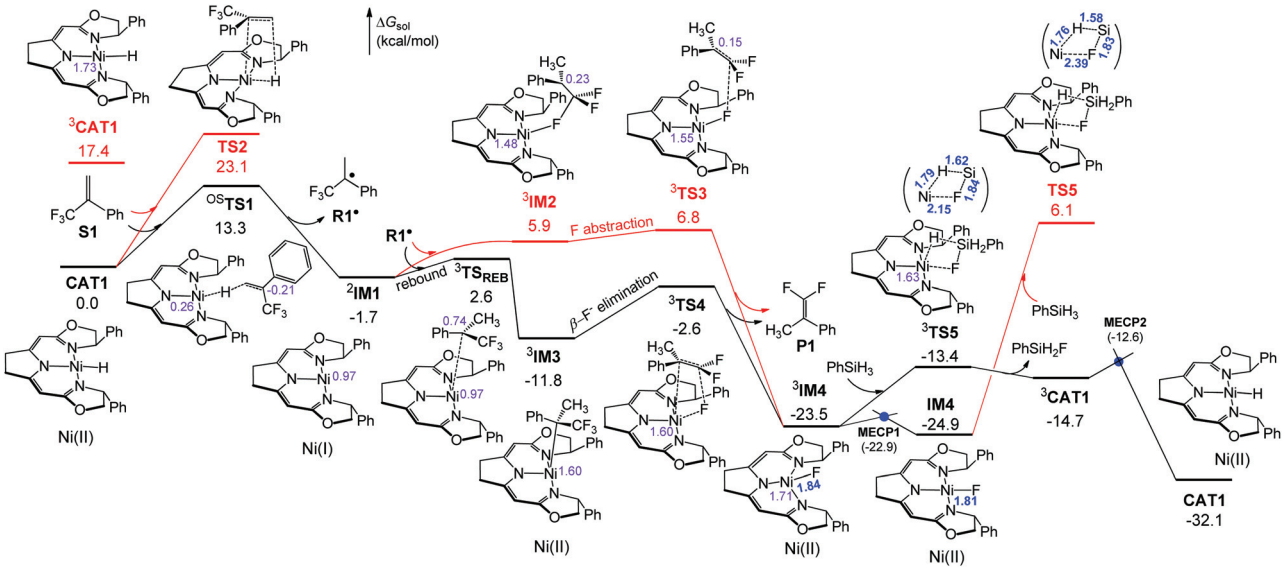

Fig. 1 Free energy profile for the Ni-catalyzed HAT-initiated hydrodefluorination computed with B3LYP-D3/6-311++G(d,p)-SDD/SMD(benzene)//B3LYP-D3/6-31G(d,p)-SDD (the same below). Upper left superscripts indicate the spin states of open-shell structures, including open-shell singlets (OS) (the same below). The numbers in the purple font on selected atoms in open-shell structures denote positive α-spin and negative β-spin densities (the same below). The numbers in blue bold font denote key bond distances (Å) in **IM4**, ^{3}**IM4**, **TS5**, and ^{3}**TS5**.

0.27 Å more to attain the singlet **TS5**. This can qualitatively explain why **TS5** is considerably higher in energy than ^{3}**TS5**. We have now established a complete HAT-initiated reaction coordinate: **CAT1** → ^{OS}**TS1** → ^{2}**IM1** → ^{3}**TS$_{REB}$** → ^{3}**IM3** → ^{3}**TS4** → ^{3}**IM4** → **IM4** → ^{3}**IM4** → ^{3}**TS5** → ^{3}**CAT1** → **CAT1** (Fig. 1). The largest energy span[17] is from **CAT1** to ^{OS}**TS1**, 13.3 kcal mol^{-1}, suggesting that the HAT to C=C is the rate-determining step in this reaction. This calculated activation barrier is consistent with the reaction temperature (25 °C). The calculations also show a large overall thermodynamic driving force for the reaction (ΔG = −32.1 kcal mol^{-1}).

The hydrodefluorination of substrate **S1** is chemoselective without giving the hydrogenation product. The experimentalists speculated that a second HAT from **CAT1** to **R1**$^{\bullet}$ could be hindered by the bulky ligand environment and hence no hydrogenation.[5] As shown in Fig. 2, we found that ^{2}**TS6**, the barrier of the second HAT, is only 11.8 kcal mol^{-1} relative to its precursors, and no significant steric repulsion is observed in the optimized structure of ^{2}**TS6**. We also located a lower-energy pathway wherein **R1**$^{\bullet}$ adds to the Ni(II)[18] complex **CAT1** to form the Ni(III) species ^{2}**IM5** from which the reductive H–R1 elimination/coupling *via* ^{2}**TS7** would lead to the formation of a hydrogenation product. Yet ^{2}**TS7** is still 2.4 kcal mol^{-1} higher than ^{3}**TS$_{REB}$**. Thus, it is the exergonic rebound of **R1**$^{\bullet}$ to ^{2}**IM1** forming ^{3}**IM3** that opens up the favorable defluorination pathway and prevents hydrogenation from occurring. Hence, we have computationally gained insight into the chemoselectivity.

With the information on the mechanism in general and the rate-determining step in particular in hand, we calculated the complete pathway of the reaction involving the aliphatic alkene substrate **S2** (Fig. S4†), which is analogous to the pathway of the aryl alkene substrate **S1**. As shown in Fig. 3, the rate-determining HAT step has a barrier‡ (^{OS}**TS8**) that is 5.7 kcal mol^{-1} higher than ^{OS}**TS1** in Fig. 1. This difference can be largely accounted for by our calculations that the benzyl radical **R1**$^{\bullet}$ resulting from ^{OS}**TS1** is 6.4 kcal mol^{-1} more stable

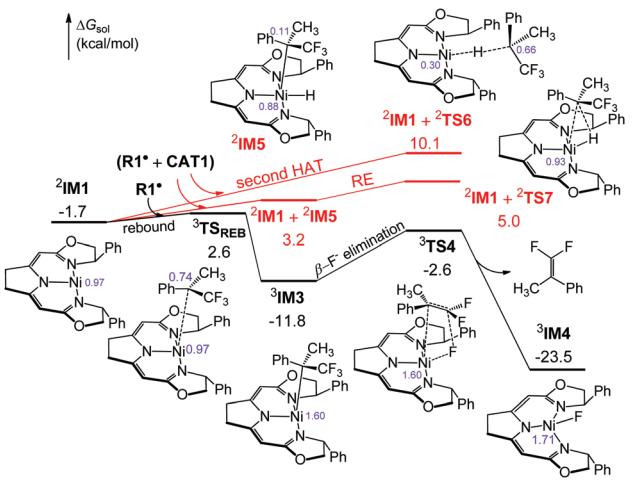

Fig. 2 Free energy profile showing the disfavored hydrogenation pathways (red) in comparison with the favored defluorination pathway (black).

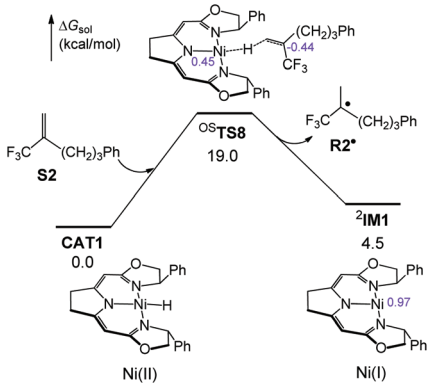

Fig. 3 Free energy profile for HAT to the aliphatic alkene **S2**.

than the alkyl radical **R2**$^{\bullet}$ from ^{OS}**TS8**. The difference of 5.7 kcal mol^{-1} ($\Delta\Delta G^{\ddagger}$) can qualitatively explain that in comparison with the **S1** reaction, the **S2** reaction would be much slower and therefore unfeasible under the experimental conditions. The computational results lend support to the experimentalists' thought that the aryl group in **S1** is essential for stabilizing the HAT-initiated carbon radical (through π resonance) because CF_3 is a radical destabilizer.

The HAT-initiated hydrodefluorination is a unique reactivity of the Ni(II) hydride complex **CAT1** bearing a weak-field N-donor ancillary ligand and does not work with metal hydrides such as $HCrCp(CO)_3$ (**CAT2**).[5] The computed profile sheds light on the lack of the hydrodefluorination reactivity of **CAT2** (Fig. 4). The HAT from **CAT2** to **S1** is endergonic by 5.3 kcal mol^{-1} due to the resultant less stable 17-electron organometallic ^{2}**IM6**. This endergonicity accounts for the higher barrier ^{OS}**TS9** *versus* ^{OS}**TS1** according to Hammond's postulate. The F abstraction barrier ^{OS}**TS10** is 27.2 kcal mol^{-1} with respect to ^{2}**IM6**, and because it makes up most of the overall barrier of 32.5 kcal mol^{-1} with respect to **CAT2**, it is the origin of why **CAT2** is unreactive towards the hydrodefluorination of **S1**. The ^{2}**IM6** to ^{OS}**TS10** barrier (27.2 kcal mol^{-1}) is higher than the analogous ^{2}**IM1** to ^{3}**TS3** barrier (8.5 kcal mol^{-1}) in Fig. 1 by 18.7 kcal mol^{-1}, which suggests the emerging Cr–F bond in ^{OS}**TS10** being weaker than the emerging Ni–F bond in ^{3}**TS3**. We calculated and compared the free energies of dissociation of the Cr–F and Ni–F bonds in the resulting fluoride complexes **IM9** and **IM4**, and the difference of 18.0 kcal mol^{-1} is very close to 18.7 kcal mol^{-1}. The β-fluoride elimination pathway through **IM7**, **IM8**, and **TS11** would be more disfavored because **TS11** is higher than ^{OS}**TS10** by 4.3 kcal mol^{-1}. The radical rebound to ^{2}**IM6** is endergonic by 11.0 kcal mol^{-1} due to the severe steric congestion in the resulting seven-coordinate **IM7** (Fig. S5†). Dissociation of a CO ligand from **IM7** is further endergonic by 2.6 kcal mol^{-1}, and the β-fluoride elimination *via* **TS11** adds another 17.9 kcal mol^{-1} to the overall barrier (this part can be attributed to the weakness of the emerging Cr–F bond in **TS11**).

Experimentally, **CAT2** shows some hydrogenation reactivity with **S1**.[5] This leads the experimentalists to envision that it

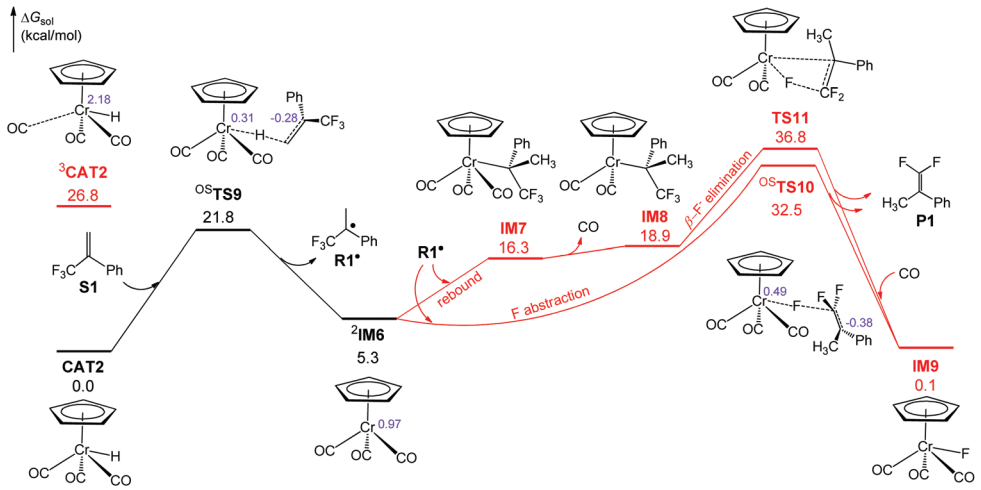

Fig. 4 Free energy profile for $HCrCp(CO)_3$ HAT-initiated hydrodefluorination.

could transfer a second hydrogen atom to **R1**•. The calculations support the experimentalists' idea (Fig. S6†).

In summary, we have performed the first computational study on a nickel hydride HAT-initiated catalytic reaction, a novel hydrodefluorination of CF_3-substituted aryl alkenes to afford *gem*-difluoroalkenes. The calculations provide detailed mechanistic insights into the reaction. The HAT step occurs *via* an open-shell singlet transition state, and the resulting carbon radical rebounds to the Ni(I) intermediate to introduce a low-energy pathway for the chemoselective β-fluoride elimination to deliver the hydrodefluorination product. The following σ-bond metathesis with the hydrosilane is enabled by a two-state reactivity of Ni(II), which regenerates the catalyst. The computations also explain why the reaction is not applicable to aliphatic alkene substrates or metal hydrides with strong-field supporting ligands such as CO and Cp. The findings of this theoretical study can have implications for developing new metal hydride HAT-initiated catalytic reactions.

Conflicts of interest

There are no conflicts to declare.

Acknowledgements

We acknowledge support for this work from the Hoffmann Institute of Advanced Materials at Shenzhen Polytechnic and the University of Colorado Denver.

Notes and references

‡Viewed alone, the barrier of ^{OS}**TS8** (19.0 kcal mol^{-1}) appears somewhat low, which is a limitation of the DFT computation. DLPNO-CCSD(T) benchmarking gives a more accurate result of 24.0 kcal mol^{-1} (Fig. S7†).

1 S. W. Crossley, C. Obradors, R. M. Martinez and R. A. Shenvi, *Chem. Rev.*, 2016, **116**, 8912–9000.
2 R. W. Hoffmann, *Chem. Soc. Rev.*, 2016, **45**, 577–583.
3 S. A. Green, S. W. M. Crossley, J. L. M. Matos, S. Vásquez-Céspedes, S. L. Shevick and R. A. Shenvi, *Acc. Chem. Res.*, 2018, **51**, 2628–2640.
4 S. L. Shevick, C. V. Wilson, S. Kotesova, D. Kim, P. L. Holland and R. A. Shenvi, *Chem. Sci.*, 2020, **11**, 12401–12422.
5 C. Yao, S. Wang, J. Norton and M. Hammond, *J. Am. Chem. Soc.*, 2020, **142**, 4793–4799.
6 (*a*) Y. Pan, J. Qiu and R. B. Silverman, *J. Med. Chem.*, 2003, **46**, 5292–5293; (*b*) S. Messaoudi, B. Tréguier, A. Hamze, O. Provot, J.-F. Peyrat, J. R. De Losada, J.-M. Liu, J. Bignon, J. Wdzieczak-Bakala, S. Thoret, J. Dubois, J.-D. Brion and M. Alami, *J. Med. Chem.*, 2009, **52**, 4538–4542; (*c*) C. Leriche, X. He, C.-w. T. Chang and H.-w. Liu, *J. Am. Chem. Soc.*, 2003, **125**, 6348–6349; (*d*) G. Magueur, B. Crousse, M. Ourévitch, D. Bonnet-Delpon and J.-P. Bégué, *J. Fluorine Chem.*, 2006, **127**, 637–642; (*e*) N. A. Meanwell, *J. Med. Chem.*, 2011, **54**, 2529–2591.
7 (*a*) M. F. Kuehnel, D. Lentz and T. Braun, *Angew. Chem., Int. Ed.*, 2013, **52**, 3328–3348; (*b*) M. K. Whittlesey and E. Peris, *ACS Catal.*, 2014, **4**, 3152–3159; (*c*) N. O. Andrella, N. Xu, B. M. Gabidullin, C. Ehm and R. T. Baker, *J. Am. Chem. Soc.*, 2019, **141**, 11506–11521.
8 B. de Bruin, W. I. Dzik, S. Li and B. B. Wayland, *Chem. Eur. J.*, 2009, **15**, 4312–4320.
9 D. Kim, S. M. W. Rahaman, B. Q. Mercado, R. Poli and P. L. Holland, *J. Am. Chem. Soc.*, 2019, **141**, 7473–7485.
10 H. Jiang, W. Lai and H. Chen, *ACS Catal.*, 2019, **9**, 6080–6086.
11 Y. Kamei, Y. Seino, Y. Yamaguchi, T. Yoshino, S. Maeda, M. Kojima and S. Matsunaga, *Nat. Commun.*, 2021, **12**, 966.
12 C. Rettenmeier, H. Wadepohl and L. H. Gade, *Chem. – Eur. J.*, 2014, **20**, 9657–9665.
13 T. Okamoto and S. Oka, *J. Org. Chem.*, 1984, **49**, 1589–1594.

14 (*a*) C. A. Rettenmeier, J. Wenz, H. Wadepohl and L. H. Gade, *Inorg. Chem.*, 2016, **55**, 8214–8224; (*b*) Y. Li, Y. Luo, L. Peng, Y. Li, B. Zhao, W. Wang, H. Pang, Y. Deng, R. Bai, Y. Lan and G. Yin, *Nat. Commun.*, 2020, **11**, 417.

15 (*a*) T. Ichitsuka, T. Fujita, T. Arita and J. Ichikawa, *Angew. Chem., Int. Ed.*, 2014, **53**, 7564–7568; (*b*) X. Zhang, Y. Liu, G. Chen, G. Pei and S. Bi, *Organometallics*, 2017, **36**, 3739–3749.

16 (*a*) D. Schröder, S. Shaik and H. Schwarz, *Acc. Chem. Res.*, 2000, **33**, 139–145; (*b*) J. N. Harvey, R. Poli and K. M. Smith, *Coord. Chem. Rev.*, 2003, **238**, 347–361.

17 (*a*) S. Kozuch and S. Shaik, *Acc. Chem. Res.*, 2011, **44**, 101–110; (*b*) S. Kozuch and S. Shaik, *J. Am. Chem. Soc.*, 2006, **128**, 3355–3365.

18 (*a*) S. Biswas and D. J. Weix, *J. Am. Chem. Soc.*, 2013, **135**, 16192–16197; (*b*) D. J. Weix, *Acc. Chem. Res.*, 2015, **48**, 1767–1775.